Synthesis of layered vs planar Mo_2C: role of Mo diffusion

2D Materials

PAPER

RECEIVED
3 November 2021

REVISED
7 December 2021

ACCEPTED FOR PUBLICATION
16 December 2021

PUBLISHED
6 January 2022

Synthesis of layered vs planar Mo_2C: role of Mo diffusion

M Arslan Shehzad[1,3], Paul Masih Das[1], Alexander C Tyner[5], Matthew Cheng[1], Yea-Shine Lee[1], P Goswami[2,5], Roberto Dos Reis[1,3], Xinqi Chen[3,6,*] and Vinayak P Dravid[1,3,4,*]

[1] Department of Material Science and Engineering, Northwestern University, Evanston, IL 60208, United States of America
[2] Department of Physics, Northwestern University, Evanston, IL 60208, United States of America
[3] Northwestern University Atomic and Nanoscale Characterization Experimental (NUANCE) Center, Northwestern University, Evanston, IL 60208, United States of America
[4] International Institute for Nanotechnology (IIN), Northwestern University, Evanston, IL 60208, United States of America
[5] Graduate Program in Applied Physics, Northwestern University, Evanston, IL 60208, United States of America
[6] Department of Mechanical Engineering, Northwestern University, Evanston, IL 60208, United States of America
[*] Authors to whom any correspondence should be addressed.

E-mail: xchen@northwestern.edu **and** v-dravid@northwestern.edu

Keywords: Mo_2C, CVD, MXenes, 2D transition metal carbides

Supplementary material for this article is available online

Abstract

Chemical vapor deposition growth of metal carbides is of great interest as this method provides large area growth of MXenes. This growth is mainly done using a melted diffusion based process; however, different morphologies in growth process is not well understood. In this work, we report deterministic synthesis of layered (non-uniform *c*-axis growth) and planar (uniform *c*-axis growth) of molybdenum carbide (Mo_2C) using a diffusion-mediated growth. Mo-diffusion limited growth mechanism is proposed where the competition between Mo and C adatoms determines the morphology of grown crystals. Difference in thickness of catalyst at the edge and center lead to enhanced Mo diffusion which plays a vital role in determining the structure of Mo_2C. The layered structures exhibit an expansion in the lattice confirmed by the presence of strain. Density functional theory shows consistent presence of strain which is dependent upon Mo diffusion during growth. This work demonstrates the importance of precise control of diffusion through the catalyst in determining the structure of Mo_2C and contributes to broader understanding of metal diffusion in growth of MXenes.

1. Introduction

Since the discovery of layered materials, i.e. graphene and transitional metal chalcogenides (TMD) [1–3], 2D materials have received wide attention in the past decade [4, 5]. Recently, 2D transition-metal carbides (TMC) have received more attention due to their outstanding electronic, magnetic, and mechanical properties and emerged as a new class of 2D-materials [3]. TMCs can be used in energy storage, catalysis, adsorption, and photoelectric applications [6, 7]. Synthesis of these 2D materials has been restricted to extraction from MAX phases where 'M' is transition metal, 'A' is an A group element, and 'X' is C and/or N. This extraction is mainly done by removal of element 'A' via the chemical etch solution, typically hydrofluoric acid or hydrochloric acid [8]. However, the end product of this technique is typically small and exhibits numerous structural defects. This is due to exposure to acids and nature of extraction process applied using this technique [9, 10].

Lately, growth of large-area and high quality 2D Mo_2C crystals has been enabled using chemical vapor deposition (CVD) [11]. These crystals exhibit attractive properties, such as 2D superconductivity, [11, 12] and magnetoresistance [13, 14]. The growth process includes use of dual substrates copper and molybdenum (Cu/Mo) and exposure to high temperatures which allows the Cu to melt. Subsequently, Mo adatoms diffuse from the melted Cu to the surface of the liquid and react with the carbon precursors from the decomposition of methane to form Mo_2C crystals [11]. Although intensive investigations have been conducted on the growth of these CVD grown materials system, the understanding of growth mechanism is still not certain [15]. It has been shown in

various studies that the melting of Cu plays an essential role in the growth mechanism of these structures [11, 16]. Furthermore several studies looked into utilizing different catalysts to grow these structures [17–20]. Similarly, it has been revealed that by controlling the carbon source, these crystals can be grown via graphene template which helps to direct these structures [15, 21]. Moreover, recently growth of layered and planar structures grown on two different Cu substrates and has been explained due to thickness dependence of Cu and inter-gliding of Mo [22, 23]. However, most of these studies have not considered or discussed sparsely the diffusion of molybdenum through Cu which also plays a vital role in determining the structure.

In this work, we report the synthesis of different structures of Mo_2C crystals, grown directly on liquid Cu. We demonstrate coexistence of two different morphologies on the liquid Cu surface. We attribute these differences in the structural characteristics can be controlled by availability of Mo during growth. Transmission electron microscopy shows an expansion in lattice of layered structures which is further explained by stress during the growth. Density functional theory (DFT) confirms that the difference in growth is dependent on the excess Mo environment which is in good agreement with the experimental results. It also confirms that Mo excess environment leads to expansion in the layered crystal structure.

2. Experimental details

The stack of molybdenum (Mo) and copper (Cu) foil is placed in alumina boat in fused quartz tube. To melt the Cu, 1090 °C is achieved under H_2 (10 sccm) and Ar (100 sccm) at the rate of 20° min^{-1} (more details below). The temperature is then dropped down to 1080 °C in 3 min for growth. CH_4 (2 sccm) is then introduced into the reaction tube at ambient pressure to initiate the growth of different 2D Mo_2C crystals. The growth time varies from 10 to 30 min to get different densities of these crystals. Atomic force microscopy (AFM), scanning electron microscopy (SEM) and scanning transmission electron microscopy (STEM) are used to see the morphology of grown structures. Raman and x-ray photoelectron spectroscopy (XPS) are used to see the atomic vibrations and elemental composition.

2.1. CVD growth and transfer

Double side polished Cu foil (Alfa Aesar, 99.5% purity, ∼10 μm thick) is cut into 5 × 5 mm^2 pieces and placed on top of a Mo foil (Alfa Aesar, 99.99% purity, ∼120 μm thick) with similar dimensions. The stack is then placed in an alumina boat which is then placed in fused quartz tube with inner diameter 22 mm. Later, the Cu/Mo substrates are heated to 1090 °C in a horizontal tube furnace (Lindberg Blue M) under H_2 (10 sccm) and Ar (100 sccm) at the rate of 20° min^{-1}. The temperature is then dropped down to 1080 °C in 3 min for growth. CH_4 (2 sccm) is then introduced into the reaction tube at ambient pressure to initiate the growth of different 2D Mo_2C crystals. The growth time varies from 10 to 30 min to get different densities of these crystals. After the reaction, the samples are cooled down to 600 °C at slower rate under Ar and H_2. After 600 °C, H_2 flow is turned off and samples are quickly removed from the high temperature to ensure rapid cooling to room temperature. Conventional transfer technique for 2D materials is used for the transfer of Mo_2C crystals [24]. A thin layer of poly(methyl methacrylate) (PMMA, A3) is first spin-coated on the surface of ultrathin α-Mo_2C crystals at 3000 rpm for 1 min and cured at 90 °C for 2 min; the PMMA-coated samples are subsequently immersed in a 0.2 M $(NH_4)_2S_2O_8$ solution at 70 °C for 10 min to etch the Cu substrate. Later, the PMMA-coated ultrathin α-Mo_2C crystals are transferred to target substrates, such as SiO_2/Si and TEM grids. Warm acetone (50 °C) is used to dissolve the PMMA layer.

2.2. Characterizations

Horiba LabRam Confocal Raman equipped with a HJY detector is used to collect Raman spectra of all samples in ambient conditions. 473 nm laser with 600 gr mm^{-1} grating and 1% ND filter is used. The Thermo Scientific ESCALAB 250Xi XPS was used to obtain the XPS spectra at room temperature using 500 μm spot size, monochromatic Al K*a* source and the spectra were calibrated relative to the carbon peak at 284.8 eV. The background subtraction was done using the Shirley method. Bruker fast scan AFM is used in tapping mode with scan rate of 20 Hz. TEM samples are prepared by transferring flakes using PMMA and conventional copper etching with $FeCl_3$. High resolution STEM and selected area electron diffraction (SAED) patterns are obtained using a JEOL ARM200CF microscope at 200 kV along the out-of-plane direction, *c*-axis, which is parallel to the [0001]-zone axis. Images are collected using either JEOL bright field (BF) (0–60 mrad) or annular dark field (ADF) (90–370 mrad) detector with a 8 μs dwell time. Errors for SAED lattice spacing are computed using the intensity FWHM for multiple sets of six-fold symmetric diffraction spots. STEM-EDS was conducted with an Oxford silicon drift detector to analyze the stoichiometry.

2.3. Computational simulations

All first-principles calculations for Mo_2C are based on DFT and were performed using the Quantum ESPRESSO software package [25, 26]. The exchange-correlation potentials use the Perdew–Burke–Ernzerhof (PBE) parameterization of the generalized gradient approximation [27]. A plane-wave cutoff of

150 Ry is used in all calculations. The primitive unit cell with $a = 4{:}754$ Å, $b = 5{:}241$ Å, and $c = 6{:}076$ Å is sampled with a k-mesh of $9 \times 8 \times 8$. Spin–orbit effects are included in calculations of electronic band structure. For adsorption energy calculations are done using the same Quantum ESPRESSO software package. The exchange-correlation potentials use the PBE parameterization of the generalized gradient approximation. A plane-wave cutoff of 50 Ry is used in all calculations. For optimization of the adsorption of Mo and C atoms, the bottom two layers of a $4 \times 1 \times 1$ supercell constructed from the primitive (conventional) unit-cell of Mo_2C(Cu) with 20 Å of vacuum in the (100) direction are held fixed. The supercells are sampled with a Monkhorst-pack grid of $1 \times 5 \times 5$.

3. Results and discussion

As explained above, the growth of Mo_2C crystals is done using Mo/Cu substrates (see details in section 2). The scheme of growth process, where Mo and Cu foils are placed on top of each other, is shown in figure 1(a). The Cu/Mo substrates are first heated to 1090 °C to melt Cu under H_2 (10 sccm) and Ar (100 sccm) and subsequently dropped to 1080 °C in 3 min for growth. Optical and cross-section SEM images of melted Cu catalyst are shown in figure S1 (available online at stacks.iop.org/2DM/9/015039/mmedia), which confirms that the surface of Cu is non-uniform. CH_4 (2 sccm) is then introduced into the reaction tube to initiate the growth of different 2D Mo_2C crystals. Different growth times of 10, 20 and 30 min give different densities of these crystals as shown in figure S2.

It has been previously shown that both nucleation density and thickness can be controlled by extending the growth time [28]. Different shapes of crystals in both types of structures are shown in figure S3. Conventional PMMA-assisted-transfer technique for 2D materials is used to transfer the Mo_2C crystals [24]. It is important to note here that extended Mo foil without Cu can impact the transfer process. Therefore, it is necessary to cut the extended Mo foil to complete a uniform transfer. Later, PMMA-coated Mo_2C crystals are transferred to target substrates, i.e. SiO_2/Si and TEM grids. Warm acetone (50 °C) is used to dissolve the PMMA for couple of hours. Transferred flakes are shown in figure S4.

As the melted Cu foil/catalyst creates a layer with inhomogeneous concentrations of Cu throughout, Mo diffusion will vary from the edge to the center surface promoting the growth of layered and planar crystals of Mo_2C as shown in figure 1. Schematics in figure 1(a) show the growth process at 1080 °C for 10 min with greater diffusion at the edges compared to surface (described in more detail in figures 3 and S9).

The difference in growth is shown in figure S5 with layered growth at the edges and planar with more consistent Cu thickness. Typical in-plane and cross section schematics of the Mo_2C structure are shown in figure 1(b) [28]. Optical images with representative schematics of both growths are shown in figures 1(c) and (d). Figure 1(c) confirms the growth of planar crystals while figure 1(d) illustrates the star-like shape of layered structures. Gradual change in optical contrast of these structures confirms the layered nature of this system. Low contrast at the edges of these structures demonstrates few layers.

To investigate the nature of these grown structures, tapping mode AFM is used. Figure 2(a) shows a topographical 4×4 μm^2 scan of a planar crystal with uniform surface and corresponding line profile, which identifies the thickness of the crystal as ∼8 nm. Figure 2(b) confirms the layered structure of grown crystals with preferential growth in the c-axis direction. The line profile exhibits distinct steps in thickness, which are attributed to different layers where edges represent mono/bilayers. To get insight on the structure of these two types of crystals, Raman spectroscopy is used. Figure 2(c) shows the spectra for both layered (in red) and planar (in black) geometries. Both spectra show typical phonon modes for Mo_2C [29]. Phonon modes at ∼143, 173 and 213 cm^{-1} correspond to B_{3g} vibrations. However, vibrations at 181, 235 and 657 cm^{-1} correspond to A_g [29]. Interestingly, there is a shift towards lower wavenumbers for the A_g mode at 653 cm^{-1} and B_{3g} mode at 141 and 170 cm^{-1} in the layered structures which can be attributed to stress in the in-plane direction. No significant change is observed on different layers confirming same crystal structure throughout the layers as shown in figure S6. To further characterize the bonds in the Mo_2C flakes, we use XPS. The obtained Mo and C spectra are shown in figure 2(d). The characteristics peaks for molybdenum and carbon around 228 and 283 eV confirm the presence of Mo–C bond. The binding energy of the Mo^{2+} peaks located at 228.3 eV ($Mo^{2+}3d_{5/2}$) and 231.5 eV ($Mo^{2+}3d_{3/2}$) are assigned to Mo–C [30]. Furthermore, the prime peaks of C 1s at 283.2 and 284.6 eV can be ascribed to Mo–C and C–C, which are the principle chemical arrangements in Mo_2C [31].

To comprehend the growth of two different crystals, it is important to understand the kinetics. Mo-diffusion limited growth mechanism is proposed where the competition between Mo and C adatoms along the edges and surfaces determines the morphology of grown crystals as explained in TMD growth [12, 32–34]. It is important to consider the difference in CVD growth schemes of TMDs and current sandwich approach. In TMDs growth mostly it is done using vaporization of metal oxide and nucleation on any secondary substrate. But in the current case, molybdenum must diffuse through the

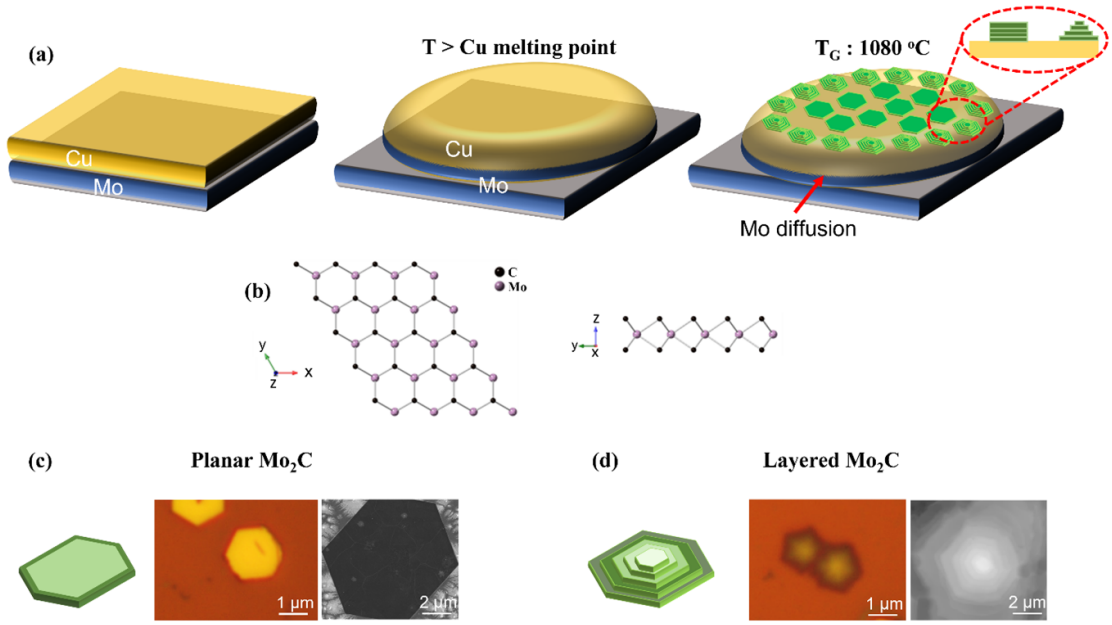

Figure 1. Scheme of experiment where Mo and Cu foils are placed on top of each other is shown in (a). To diffuse Mo through the copper, Cu foil is heated above the melting temperature. Due to inhomogeneous surface coverage of Cu throughout the surface, Mo diffusion varies from edge to surface which leads to layered and planar crystals of Mo_2C. Schematics show the growth process at 1080 °C for 10 min with more diffusion at the edges compared to surface. Typical structure of Mo_2C is shown in (b). Optical and SEM images of resulting structures are shown in figures (c) and (d). Figure (c) shows the growth of planar crystals while (d) confirms star-like shape of layered structures.

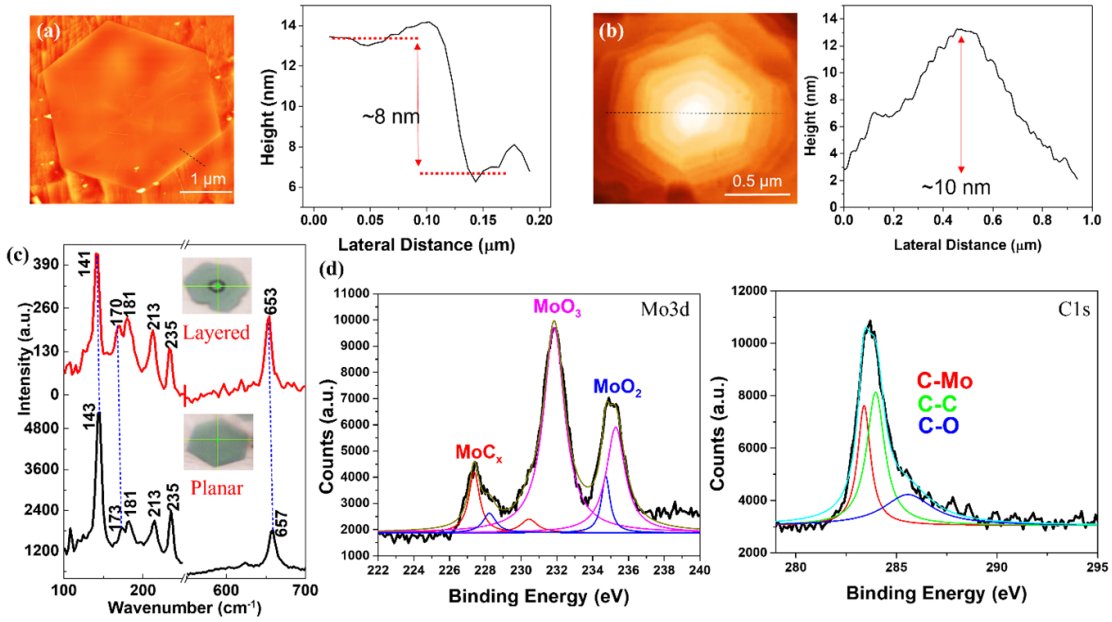

Figure 2. AFM in tapping mode is used to determine the topography of grown structures. Figure (a) shows topographical image of planar crystal with line profile which confirms the thickness of the crystal as ∼8 nm. Figure (b) confirms the layered structure of grown crystals with line profile corresponding to distinct steps in the thickness, representing different layers with thickness of 10 nm. Raman is used to determine phonon vibrations. Figure (c) shows spectra for both layered (in red) and planar (in black) structures. Both spectra show typical phonon modes for Mo_2C. Phonon modes at ∼140, 170 and 213 cm^{-1} correspond to B_{3g} vibrations while those at 180, 235 and 650 cm^{-1} correspond to Ag. The presence of Mo–C bond is confirmed by XPS, Mo and C spectra is shown in figure (d).

catalyst in its melting form to crystalize on the surface. Essence of melting is further confirmed by reducing the growth temperature below the melting point of copper where growth was not successful as shown in figure S14. Schematic of growth mechanism is shown in figure 3(a). Upon melting the copper its surface will decompose H_2 and CH_4 to give excess hydrogen environment. This excess hydrogen/Cu surface will

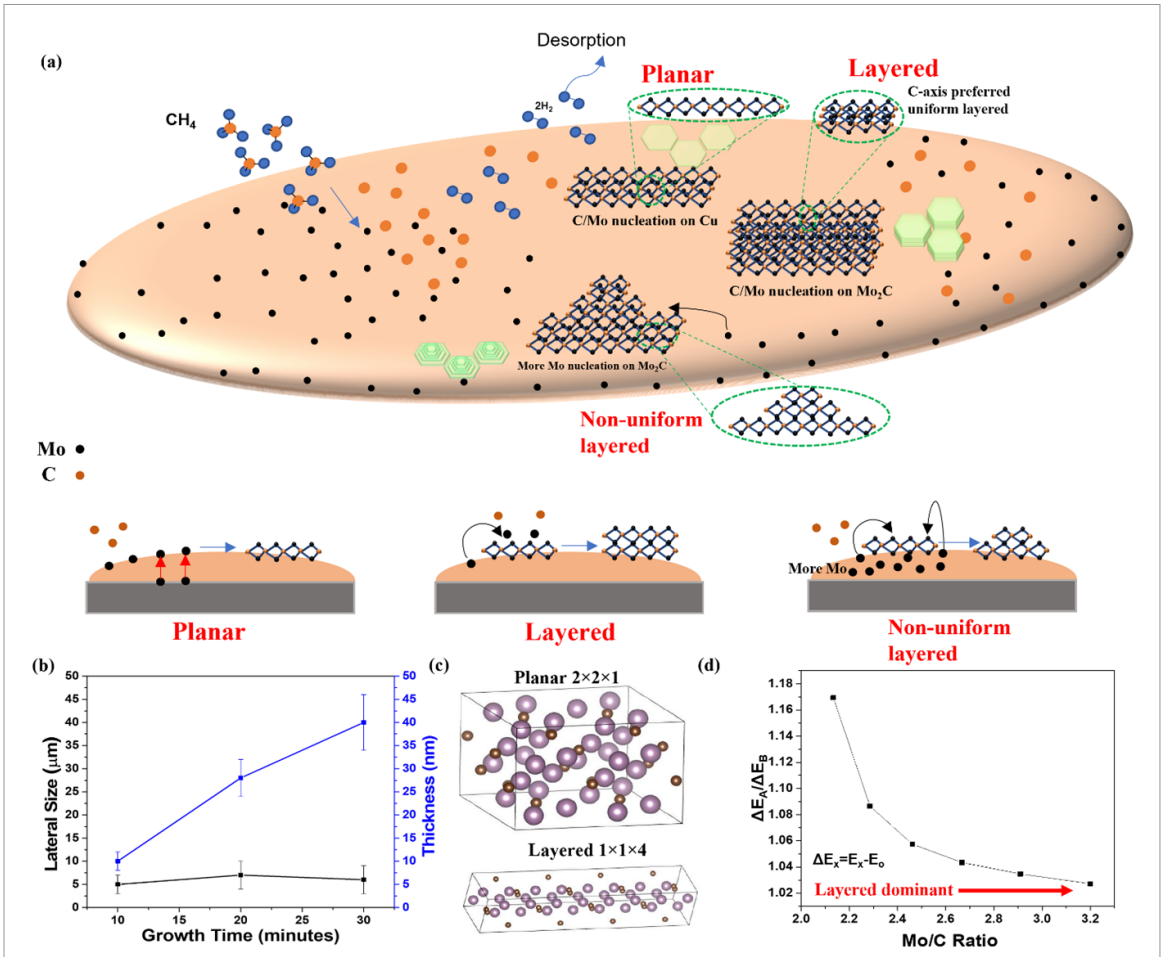

Figure 3. Schematics of growth in two different cases is shown in (a). Time dependent growth is done as shown in figure S2, thickness and lateral size relation is shown in (b). Two Mo_2C supercells of dimension planar $1 \times 2 \times 2$ and layered $4 \times 1 \times 1$, as supercells A and B, respectively, are shown in figure (c). Upon addition of 20 Å vacuum along the (100) direction, supercell A simulates the ultra-thin limit, and supercell B simulates the layered Mo_2C. (d) Deviation of total energy for supercells A and B, from the maximally stable configuration as a function of the Mo to C ratio. As this ratio deviates from the ideal value of 2.0, the layered compound becomes energetically favorable.

act as a diffusion promoter. Mo atom from the molybdenum foil will diffuse through the molten Cu to the surface. Methane provides carbon source which then will react with incoming Mo adatoms and nucleate to form Mo_2C crystals. Considering the atomic ratio of Mo_2C, steady Mo diffusion is required to get symmetric growth. However, it is important to consider the adsorption energy of already grown crystals. The adsorption energy of X (X = Mo or C) on the surface of M (M = Cu (111) or Mo_2C (100)) is defined as follows:

$$E_{ads}^{X,M} = E(M+X) - (E(X) + E(M)). \qquad (1)$$

It is observed that adsorption energy for Mo ($E_{ads}^{Mo,Cu}$) and C ($E_{ads}^{C,Cu}$) on Cu is 0.419 Ry and 0.187 Ry. Contrary to this, a favorable adsorption energy is found for Mo (E_{ads}^{Mo,Mo_2C}) and C (E_{ads}^{C,Mo_2C}) on Mo_2C as −0.69 Ry and −0.59 Ry, respectively. Schematics of adsorption is shown in figure S7. These calculations suggest that it is energetically favorable for Mo/C to adsorb onto the surface of Mo_2C compared to Cu, favoring a *c*-axis preferable growth of Mo_2C. As a result, once there is enough lateral growth of Mo_2C, it prefers to crystallize on Mo_2C surface shown in schematics. To confirm this, time dependent growth is done as shown in figure S2. Figure 3(b) shows a correlation of thickness and lateral growth with time. A linear increase in thickness is observed with elevated times. Contrary to this, lateral distance of grown crystals was consistent (∼6 μm) throughout all growths which supports our results. Due to abundance of Mo upon melting of Cu, edges of Cu will have more Mo concentration which lead to uneven distribution of C and Mo. To confirm this, cross-section EDX scan is used to see the elemental composition at the edge and center of melted foil shown in figure S8. Furthermore, EDX point analysis from edge to center show a decay in the Mo presence which further confirms the presence of abundant Mo on the edges.

It is evident from adsorption energy calculations that Mo adsorption on Mo_2C (E_{ads}^{Mo,Mo_2C}) is more favorable than C on Mo_2C (E_{ads}^{C,Mo_2C}). As a result of increase in Mo, it prefers to nucleate on already grown Mo_2C surface which leads to more *c*-axis preference as shown in figure 3(a). To determine whether the

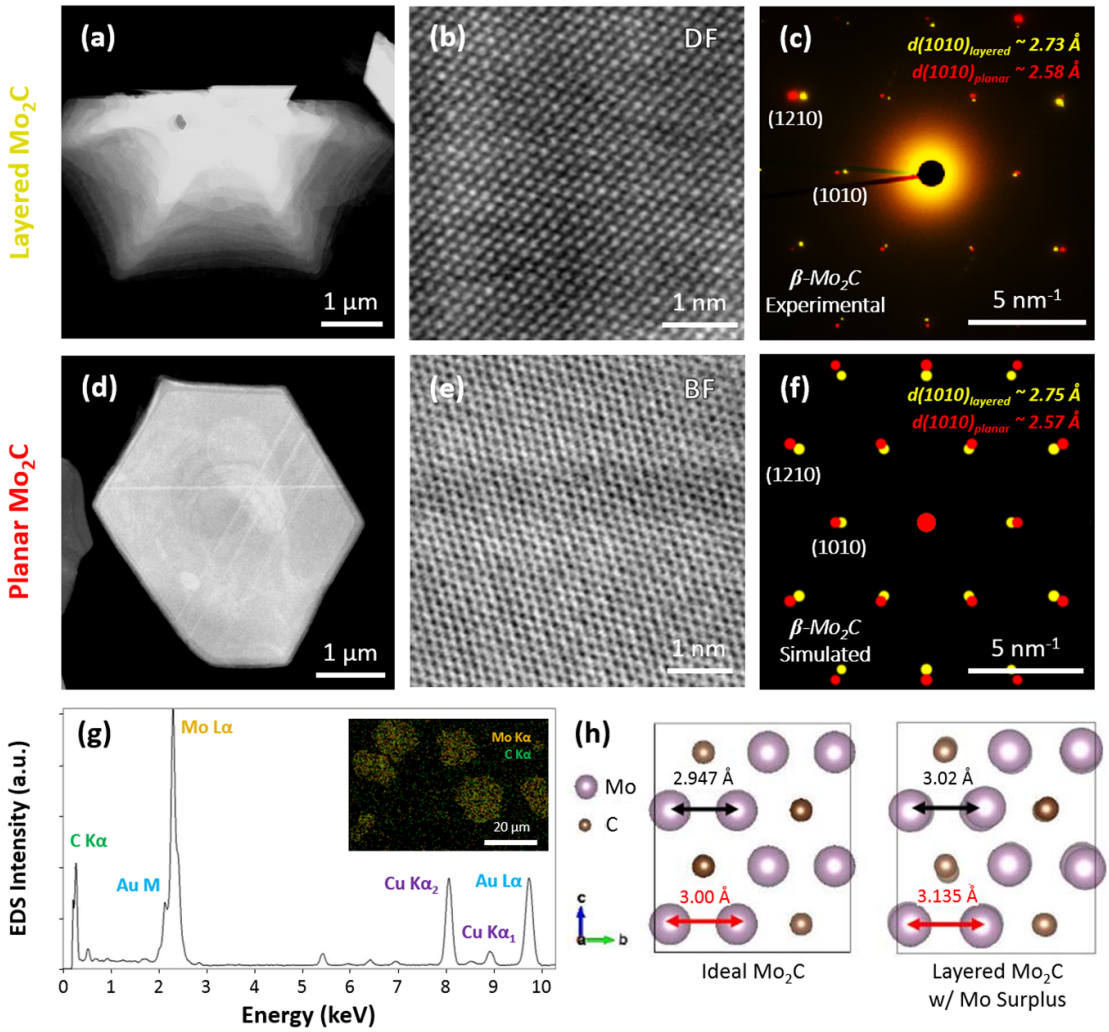

Figure 4. Low resolution STEM images of layered and planar structure are shown in figures 3(a) and (d). High resolution BF and DF images for layered and planar structure confirm the single crystalline nature of both structures shown in (b) and (e). Interestingly, SAED patterns show difference in the atomic lattice of the two structures shown in figure (c). Expanded atomic lattice of 2.72 Å of layered structure is observed compared to 2.58 Å in planar structure. This expansion in the lattices is in good agreement with simulated structure shown in (f). Furthermore, EDS map and spectra verify the presence of Mo and C elements as seen in figure (g). (h) DFT simulation is used to confirm the presence of strain in Mo excess environment. Relaxed supercell with ratio, Mo/C = 2.1 (32/15), exhibits greater in-plane lattice spacing (h).

planar or layered system is favorable under conditions of surplus Mo, two Mo_2C supercells are considered via DFT calculations. We refer to these two supercells of dimension $1 \times 2 \times 2$ (planar) and $4 \times 1 \times 1$ (layered), as supercells A and B respectively as shown in figure 3(c). Upon addition of 20 Å vacuum along the (100) direction, supercell A simulates the planar structure, and supercell B simulates the layered structure. After an initial relaxation calculation, a carbon vacancy is induced to simulate an environment with surplus Mo and the systems is relaxed again.

This procedure is repeated to simulate environments of increasing Mo abundance with the total energy of supercells A and B, E_A and E_B respectively, measured after each relaxation. As expected, the layered system is energetically favored by 2.563 Ry for a system with ideal ratio Mo/C = 2.0. We use the total energy of this structure to set a reference energy, E_0. Deviation from E_0 in supercells A and B as a function of the ratio Mo/C is then quantified. The results shown in figure 3(c) demonstrate that, as the abundance of Mo is increased, the layered structure is energetically favorable. As more carbon vacancies are induced the degree by which this structure is favored decreases due to the crystal being increasingly likely to break apart.

Previously, we have seen a direct relation of diffusion on thickness of catalyst in different materials systems [35, 36]. Similarly, it is known that melting temperature of catalyst drop significantly by reducing the size which impact diffusion and activation energy (E_a) [37]. Considering the lateral thickness of catalyst varies from center to the edge, there can be a drop in the melting temperature. Activation energy of the system can be addressed as:

$$E_a = n\Delta S_n T_c \tag{2}$$

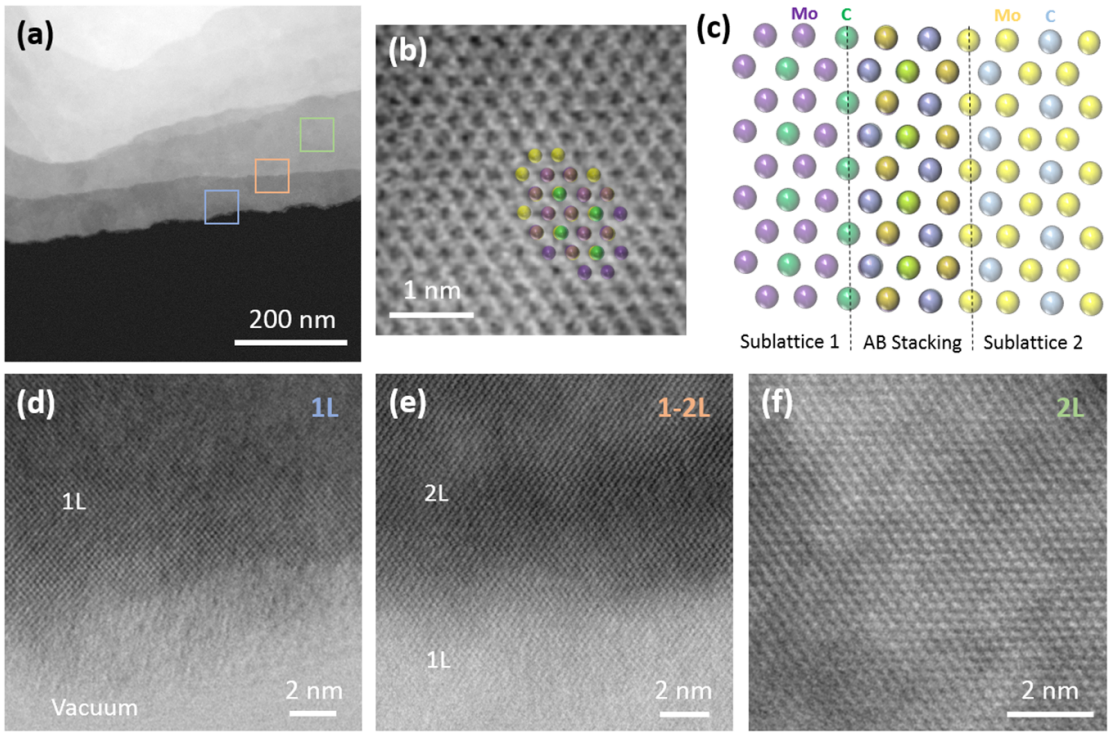

Figure 5. (a) Low magnification atomic-resolution STEM-ADF image showing steps ranging from mono to multiple layers in layered Mo_2C crystals. Figure (b) shows atom-resolved stacking variations in mono, bilayer and interface of both highlighted in blue, orange and green boxes in (a). Layer numbers are assigned based on the ADF contrast from the edge of the flake. A schematic of interface of mono and bilayer is shown in figure 5(c). Figures (d)–(f) show high resolution images of mono layer, interface of mono and bilayer, and bilayer, respectively.

where n can be considered as 12.8 for vacancy exchange mechanism [38], ΔS_n is the melting entropy of the Mo_2C and T_c is the growth temperature. In our case, melting entropy is different for bulk (center) and thin (edges) catalyst and can be adopted as:

$$\Delta S_n = \Delta S_b + \frac{3R}{2} ln \frac{T_{\mathrm{m,thin}}}{T_{\mathrm{m,bulk}}}. \qquad (3)$$

Here, ΔS_b is the entropy of bulk Mo_2C and is considered 12.95 [39], R is the gas constant. $T_{\mathrm{m,bulk}}$ and $T_{\mathrm{m,thin}}$ are the melting temperature of bulk and thin catalyst. Melting temperature of Bulk Cu is 1358 K however, by changing the catalyst thickness it can drop. Figure S9(a) show the relationship between entropy and change in melting temperature ($T_{\mathrm{m,thin}}$). It also confirms that thinner catalyst can lead to decrease entropy of the system. Moreover, linear correlation between activation energy and entropy confirms that thinner catalyst size can lead to lower activation energy. This implies lower activation energy at the edges which leads to higher diffusion and ultimately more layered dominant growth.

For an in-depth structural analysis, high resolution STEM (HR-STEM) is used. Low magnification STEM images of the layered and planar structures are shown in figures 4(a) and (d). Atomic resolution BF and ADF images (see details in section 2) for layered and planar structures confirm the hexagonal single crystal nature of both as shown in figures 4(b) and (e). Interestingly, SAED patterns show a difference in the atomic lattice between the two structures shown in figure 4(c). For example, the layered configuration exhibits a (1010) lattice spacing of 2.73 (±0.04) Å, while the corresponding (1010) spacing in the planar structure is 2.58 (±0.04) Å. This expansion can be due to the stress caused by higher diffusion of Mo at the edges as already confirmed by Raman. Similarly, expansion in lattices is in good agreement with simulated structure shown in (f). To confirm the presence of strain, we calculated the distance between adjacent Mo atoms following the relaxation calculation performed in the Mo abundant environment and the crystal structure is observed and compared to the ideal system in figure 4(h). The corresponding lattice values of planar surface in the ideal case is 2.947 Å and 3.0 Å. The small difference indicates that the strain does not exist on the surface of these Mo_2C flakes. Contrary to this, the layered surface is stretched by 1.5% as compared with the planar surface. As a result, the corresponding modulation of layered crystals is much more obvious than the planar counterpart. This is in alignment with the experimental observations. Energy-dispersive x-ray spectroscopy (EDS) map and spectra confirm the presence of Mo and C as seen in figure 4(g). EDS and SIMS maps also indicate distinct elemental distributions as shown in figures S10 and S11.

As confirmed previously, the planar structures show flat surfaces without any variations. In contrast, a significant periodic modulation of the lattice is observed in layered structures. It is known that melted Cu based growth can lead to strain and defects during the growth process [15]. It is apparent that the strain present in the layered structures is closely related to the observed modulation, where lattice stretching is directly indicative of strain. The more the lattice is stretched, the stronger the periodic lattice modulation will be. Most studies consider this strain in the structure, undesirable [40]. However, we propose that controlling these strains can help control the 2D growth of these structures, which is one of the major challenge in this area since MXenes prefer to grow along the *c*-axis. Figure 5 shows atomic-resolution ADF-STEM images of steps ranging from mono to multiple layers in the layered system. Figure 5(b) shows atom-resolved stacking variations in mono, bilayer, and interface of both highlighted in blue, orange and green boxes in figure 5(a). Schematic of interface of mono and bilayer is shown in figure 5(c). Figures 5(d) and (f) show high resolution images of mono layer, interface of mono and bilayer, and bilayer, respectively. Photoluminescence (PL) spectra is taken on both types of structures shown in figure S13. Both structures showed emission at the 590 nm however interestingly, a strong increase in the emission from layered structures showed presence of defects on the layered system. This enhancement can be vital to use these materials in electronic and other optoelectronic applications. Moreover, DFT is used to determine the band structure in both cases and is shown in figure S12. It is important to note the increased density of states in the vicinity of the Fermi energy. As Mo_2C is previously found as a potential candidate for superconducting applications we believe an increase in density of states near the Fermi energy has the potential to improve such applications.

To conclude, we demonstrate coexistence of two different morphologies on the catalyst which is attributed due to differences in Mo diffusion through irregular thickness of catalyst. An expansion in lattice of layered structures confirms the presence of stress during the growth. Theoretical calculations confirm that the difference in growth is dependent on the excess Mo environment which is in good agreement with the experimental results.

4. Summary and conclusions

Herein we report controlled growth of large scale Mo_2C crystals, directly on liquid Cu. We observe coexistence of two different morphologies on the liquid Cu surface. These growth variations are explained due to difference in molybdenum diffusion through the melted catalyst. Layered structures show an expansion in the lattice which is further confirmed by the presence of strain in these structures by HRSTEM and Raman. DFT corroborates that the layered structure is more favorable in Mo excess environment and in agreement with the experimental results. This study contributes to broader understanding of role of metal diffusion and demonstrates the importance of precise control of diffusion through the catalyst in determining the structure of Mo_2C.

Data availability statement

All data that support the findings of this study are included within the article (and any supplementary files).

Acknowledgments

This work was supported by NSF Division of Material Research (NSF Grant DMR-1929356). This work made use of the KECK II, EPIC and SPID facility of Northwestern University's NUANCE Center, which has received support from the SHyNE Resource (NSF Grant ECCS-2025633), Northwestern's MRSEC program (NSF Grant DMR-1720139), the Keck Foundation, and the State of Illinois through IIN. Support from the superconducting quantum materials and systems center (SQMS) (Grant DE-AC02-07CH11359) is also acknowledged. A T and P G were supported by the National Science Foundation MRSEC program (DMR-1720139) at the Materials Research Center of Northwestern University.

Conflicts of interest

These authors respectfully declare no conflicts of interest to acknowledge for this research.

ORCID iDs

M Arslan Shehzad https://orcid.org/0000-0002-6260-5764
Yea-Shine Lee https://orcid.org/0000-0002-2087-4886
Xinqi Chen https://orcid.org/0000-0003-0413-4893

References

[1] Novoselov K S, Geim A K, Morozov S V, Jiang D, Zhang Y, Dubonos S V, Grigorieva I V and Firsov A A 2004 Electric field effect in atomically thin carbon films *Science* **306** 666–9
[2] Castro Neto A H, Guinea F, Peres N M R, Novoselov K S and Geim A K 2009 The electronic properties of graphene *Rev. Mod. Phys.* **81** 109–62
[3] Novoselov K S, Geim A K, Morozov S V, Jiang D, Katsnelson M I, Grigorieva I V, Dubonos S V and Firsov A A 2005 Two-dimensional gas of massless Dirac fermions in graphene *Nature* **438** 197–200
[4] Novoselov K S, Mishchenko A, Carvalho A and Neto A H C 2016 2D materials and van der Waals heterostructures *Science* **353** 6298

[5] Fiori G, Bonaccorso F, Iannaccone G, Palacios T, Neumaier D, Seabaugh A, Banerjee S K and Colombo L 2014 Electronics based on two-dimensional materials *Nat. Nanotechnol.* **9** 768–79
[6] Anasori B, Lukatskaya M R and Gogotsi Y 2017 2D metal carbides and nitrides (MXenes) for energy storage *Nat. Rev. Mater.* **2** 16098
[7] Khazaei M, Arai M, Sasaki T, Chung C-Y, Venkataramanan N S, Estili M, Sakka Y and Kawazoe Y 2013 Novel electronic and magnetic properties of two-dimensional transition metal carbides and nitrides *Adv. Funct. Mater.* **23** 2185–92
[8] Naguib M, Mashtalir O, Carle J, Presser V, Lu J, Hultman L, Gogotsi Y and Barsoum M W 2012 Two-dimensional transition metal carbides *ACS Nano* **6** 1322–31
[9] Lukatskaya M R, Mashtalir O, Ren C E, Dall'Agnese Y, Rozier P, Taberna P L, Naguib M, Simon P, Barsoum M W and Gogotsi Y 2013 Cation intercalation and high volumetric capacitance of two-dimensional titanium carbide *Science* **341** 1502–5
[10] Naguib M, Mochalin V N, Barsoum M W and Gogotsi Y 2014 25th anniversary article: MXenes: a new family of two-dimensional materials *Adv. Mater.* **26** 992–1005
[11] Xu C, Wang L, Liu Z, Chen L, Guo J, Kang N, Ma X L, Cheng H M and Ren W 2015 Large-area high-quality 2D ultrathin Mo_2C superconducting crystals *Nat. Mater.* **14** 1135–41
[12] Geng D *et al* 2016 Controlled growth of ultrathin Mo_2C superconducting crystals on liquid Cu surface *2D Mater.* **4** 011012
[13] Song S, Wang L, Xu C, Cheng H, Ren W and Kang N 2017 Magnetotransport in ultrathin 2D superconducting Mo_2C crystals *IEEE Trans. Magn.* **53** 1–4
[14] Liu Z, Xu C, Kang N, Wang L, Jiang Y, Du J, Liu Y, Ma X L, Cheng H M and Ren W 2016 Unique domain structure of two-dimensional alpha-Mo_2C superconducting crystals *Nano Lett.* **16** 4243–50
[15] Geng D, Zhao X, Chen Z, Sun W, Fu W, Chen J, Liu W, Zhou W and Loh K P 2017 Direct synthesis of large-area 2D Mo_2C on *in situ* grown graphene *Adv. Mater.* **29** 1700072
[16] Xu C, Song S, Liu Z, Chen L, Wang L, Fan D, Kang N, Ma X, Cheng H M and Ren W 2017 Strongly coupled high-quality graphene/2D superconducting Mo_2C vertical heterostructures with aligned orientation *ACS Nano* **11** 5906–14
[17] Chaitoglou S, Giannakopoulou T, Speliotis T, Vavouliotis A, Trapalis C and Dimoulas A 2019 Mo_2C/graphene heterostructures: low temperature chemical vapor deposition on liquid bimetallic Sn–Cu and hydrogen evolution reaction electrocatalytic properties *Nanotechnology* **30** 125401
[18] Young K T, Smith C, Hitchcock D A, Walters T, Voigt C and Vogel E M 2020 The synthesis mechanism of Mo_2C on Ag–Cu alloy substrates by chemical vapor deposition and the impact of substrate choice *2D Mater.* **7** 035022
[19] Young K T, Smith C, Hitchcock D A and Vogel E M 2020 In–Cu alloy substrates for low-temperature chemical vapor deposition of Mo_2C *J. Vac. Sci. Technol.* A **39** 012201
[20] Caylan O R and Cambaz Buke G 2021 Low-temperature synthesis and growth model of thin Mo_2C crystals on indium *Sci. Rep.* **11** 8247
[21] Chaitoglou S, Tsipas P, Speliotis T, Kordas G, Vavouliotis A and Dimoulas A 2018 Insight and control of the chemical vapor deposition growth parameters and morphological characteristics of graphene/Mo_2C heterostructures over liquid catalyst *J. Cryst. Growth* **495** 46–53
[22] Zhao X, Sun W, Geng D, Fu W, Dan J, Xie Y, Kent P R C, Zhou W, Pennycook S J and Loh K P 2019 Edge segregated polymorphism in 2D molybdenum carbide *Adv. Mater.* **31** e1808343
[23] Li L, Gao M and Shi D 2019 Concentric advancing front corrugations and multiple ordered growth of 2D Mo_2C crystals *Cryst. Growth Des.* **19** 3097–102
[24] Suk J W, Kitt A, Magnuson C W, Hao Y, Ahmed S, An J, Swan A K, Goldberg B B and Ruoff R S 2011 Transfer of CVD-grown monolayer graphene onto arbitrary substrates *ACS Nano* **5** 6916–24
[25] Kresse G and Furthmuller J 1996 Efficient iterative schemes for *ab initio* total-energy calculations using a plane-wave basis set *Phys. Rev.* B **54** 11169–86
[26] Giannozzi P *et al* 2020 Quantum ESPRESSO toward the exascale *J. Chem. Phys.* **152** 154105
[27] Perdew J P, Burke K and Ernzerhof M 1996 Generalized gradient approximation made simple *Phys. Rev. Lett.* **77** 3865–8
[28] Geng D C *et al* 2017 Controlled growth of ultrathin Mo_2C superconducting crystals on liquid Cu surface *2D Mater.* **4** 011012
[29] Li T S, Luo W J, Kitadai H, Wang X Z and Ling X 2019 Probing the domain architecture in 2D alpha-Mo_2C via polarized raman spectroscopy *Adv. Mater.* **31** 1807160
[30] Cheng H, Ding L-X, Chen G-F, Zhang L, Xue J and Wang H 2018 Molybdenum carbide nanodots enable efficient electrocatalytic nitrogen fixation under ambient conditions *Adv. Mater.* **30** 1803694
[31] Ba K, Wang G, Ye T, Wang X, Sun Y, Liu H, Hu A, Li Z and Sun Z 2020 Single faceted two-dimensional Mo_2C electrocatalyst for highly efficient nitrogen fixation *ACS Catal.* **10** 7864–70
[32] Shi J *et al* 2015 Substrate facet effect on the growth of monolayer MoS_2 on Au foils *ACS Nano* **9** 4017–25
[33] Li D, Li Z, Chen P, Pi L, Zuo N, Peng Q, Zhou X and Zhai T 2021 Two-dimensional metal chalcogenide heterostructures: designed growth and emerging novel applications *Adv. Mater. Interfaces* **8** 2100515
[34] Zhang T *et al* 2016 Twinned growth behaviour of two-dimensional materials *Nat. Commun.* **7** 13911
[35] Rehman S, Hafeez M, Manzoor U, Khan M A and Bhatti A S 2012 Competitive role of Mn diffusion with growth in Mn catalyzed nanostructures *J. Appl. Phys.* **111** 084301
[36] Rehman S, Shehzad M A, Hafeez M and Bhatti A S 2014 Essential role of catalysts (Mn, Au, and Sn) in the vapor liquid solid growth kinematics of ZnS nanowires *J. Appl. Phys.* **115** 024312
[37] Safaei A and Shandiz M A 2009 Size-dependent thermal stability and the smallest nanocrystal *Physica* E **41** 359–64
[38] Gorshkov A V 2000 Empirical relation for the activation energy of diffusion in elemental substances *Inorg. Mater.* **36** 22–23
[39] Rumble J, Lide D and Macdonald F 2018 Chemical safety data in the handbook of chemistry and physics *Abstr. Pap. Am. Chem. Soc.* vol 255 (CRC Handbook of Chemistry and Physics) p 470 (available at: http://webdelprofesor.ula.ve/ciencias/isolda/libros/handbook.pdf)
[40] Qiao J-B *et al* 2017 One-step synthesis of van der Waals heterostructures of graphene and two-dimensional superconducting Mo_2C *Phys. Rev.* B **95** 201403